Fermi National Accelerator Laboratory

Summer Internship 2018 - Final Report

Digital Phase Comparator for the characterization of a Superconductive Quantum System

Author:
Fabio Bosco

Supervisors:
Silvia Zorzetti
Roman Pilipenko
Danil Frolov

09/26/2018

Abstract

The assigned task requires to investigate some features of a quantum system by performing repeated measures. The features that we want to observe are physically related to the phase shift that an injected signal experiences when transmitted through the system itself. Thus a system to achieve this phase difference measurement has been designed, implemented and tested. Quantum systems usually require several measurements and statistical analysis to be applied therefore a digital system has been developed letting the acquired data being processed fast. In this report a brief introduction on Quantum Computing is brought followed by an overview of the physical properties under investigation. Then the design of the digital system is explained showing the results achieved testing its main blocks. Both the successful results and the drawbacks of the system are highlighted.

Contents

1 Physics Overview

At Fermilab the *Applied Physics and Superconductive Technology Division* is working on the SRF program, which stands for Superconductive Radio Frequency. Many scientists from different countries in the world are involved in this project to realize radio frequency cavities having some of the highest quality factors ever, approaching values of $Q \approx 10^{11}$. These type of cavities are designed to be one of the main components of the linear accelerators that will be operating for the PIP-II and LCLS-II projects. The former, *Proton Improvement Plan*-II, is going to achieve high intensity proton beams provided to those experiments at Fermilab that require them while the latter, *Linac Coherent Light Source*-II, will generate hard X-Ray pulses in a free-electron laser at SLAC in California.

One further project involving superconductive cavities is Quantum. Fermilab is progressing in the innovative field of Quantum Computing thanks to the strong collaboration among material scientists, physicists and engineers. Here SRF cavities are used to build resonators that are coupled to a *qubit* achieving the building block for quantum information.

1.1 Quantum Computing

Quantum Computing deals with information storage and processing as well as its classical counterpart. However, what makes quantum computing different is that the information is carried by a quantum physical system called *qubit* [1]. A quibit can basically be any two energy level quantum system whose eigenstates are referred to as $|0\rangle$ and $|1\rangle$. Unlike the classical bit, which only assumes 'low' *or* 'high' value, quantum mechanics allows the qubit to exist in a superposition of its eigenstates. This property gives rise to the main advantages and peculiarities of quantum computing which open to new surprising possibilities.[1]Hence the quibit is described by a state function that takes the form

$$|\psi\rangle = \alpha\,|0\rangle + \beta\,|1\rangle \qquad\qquad \alpha, \beta \in \mathbb{C}. \tag{1}$$

Since a normalization for the state vector belonging to the Hilbert space is applied, such that

$$\langle\psi|\psi\rangle = |\alpha|^2 + |\beta|^2 = 1, \tag{2}$$

the state function can be represented as a vector whose arrow lies on a sphere having unit radius called *Bloch Sphere*. The degrees of freedom arising form this

[1] "Nature is quantum, goddamn it! So if we want to simulate it, we need a quantum computer." Richard Feynman.

representation are understood once normalization is taken into account and a suitable coordinate change, due to arbitrariness, is introduced so that

$$\alpha = \cos\frac{\theta}{2}, \qquad \beta = e^{i\varphi}\sin\frac{\theta}{2}, \tag{3}$$

where $\theta \in [0, \pi]$ and $\varphi \in [0, 2\pi)$. The expression in (3) is derived using a representation known as Hopf coordinates.

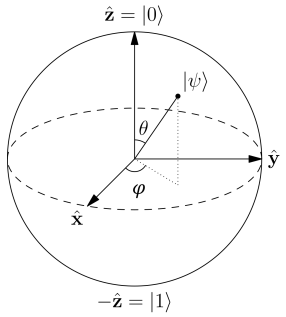

Figure 1: Bloch Sphere Representation.

Since the only result of a precise measurement for a given dynamical observable is one of the eigenvalues of the corresponding operator [2] and (2) holds, the complex coefficients α and β are to be considered probability amplitude with their square magnitude being the probability that the state is found to be, respectively, $|0\rangle$ or $|1\rangle$ after that observable has been measured.

Quantum computing brings several advantages with respect to classical computing, most of them being related to the possibility of having superposable states. First the information carried by a set made by, say, n qubits grows exponentially since they allow simultaneous operation with the 2^n eigenstates, each of them being weighted by a complex probability amplitude coefficient. A classical set of n bits would be found to be only one of those states described by n coefficients. This features implies also that parallel computation is achievable allowing higher speed for a given algorithm. Further advantages of quantum computing do not possess any classical counterpart being related to purely quantum features. The main ones, the *interference* and the *entanglement*, can occur to the wave function that describes the state of the qubit.

1.2 Superconductive Qubit

In superconductive technology the qubit can be achieved by means of a nonlinear resonant structure made of superconductive material. This structure is known as *Josephson Junction*. When brought at low temperatures the electrons in a metal form pairs that move together behaving as a single bounded particle with integer spin. These bosons experience very low resistance when moving inside the

metal giving rise to the class of material called superconductors. Cooper pairs are responsible for the supercurrent that flows by quantum tunneling through the thin layer of insulator, often referred to as weak connection, between the superconductive metal stripes of the Josephson junction.

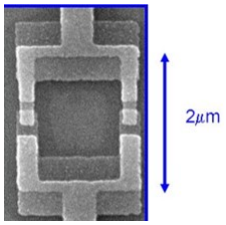

(a) Josephson Junction.

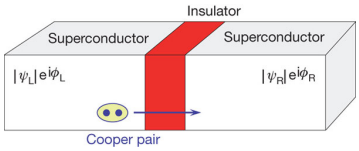

(b) Cooper pair flow.

Figure 2: Qubit in superconductive technology.

A linear resonant circuit behaves just like an harmonic oscillator [2], its Hamiltonian being

$$H = \frac{\Phi^2}{2L} + \frac{Q^2}{2C}, \tag{4}$$

where Φ is the magnetic flux through the inductance and Q is the charge stored in the capacitor. Thus it possess infinite equally spaced energy levels $E_n = \hbar\omega_0(n+\frac{1}{2})$ separated by an amount of $\hbar\omega_0$ where $\omega_0 = \frac{1}{\sqrt{LC}}$. The uniform spacing does not allow to identify the $|0\rangle$ to $|1\rangle$ transitions uniquely which is necessary to build a qubit. This problem is overcome using the Josephson junction that is still a resonator but whose inductance has a nonlinear dependence on the magnetic flux introducing separation among the energy values [3].

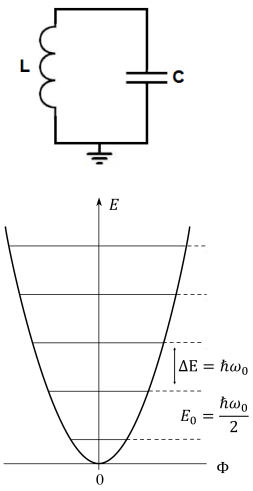

(a) Linear Resonator.

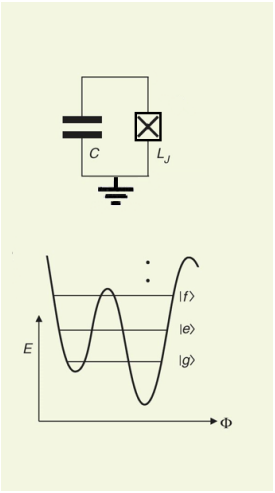

(b) Nonlinear Resonator.

Figure 3: Circuit symbol and energy values for a resonator.

Once accomplished the qubit is hang inside a resonant RF cavity whose walls are made of superconductive material. The overall system is thus made of two coupled resonator. Among the main consequences of this coupling one is the shift of the resonant frequency of the cavity mode due to the qubit. When the input power injected in the cavity is decreased the cavity behaves in the quantum regime so that the interaction with the qubit affects its hamiltonian causing a detuning of the resonant frequency known as *Dispersive Shift* [4].

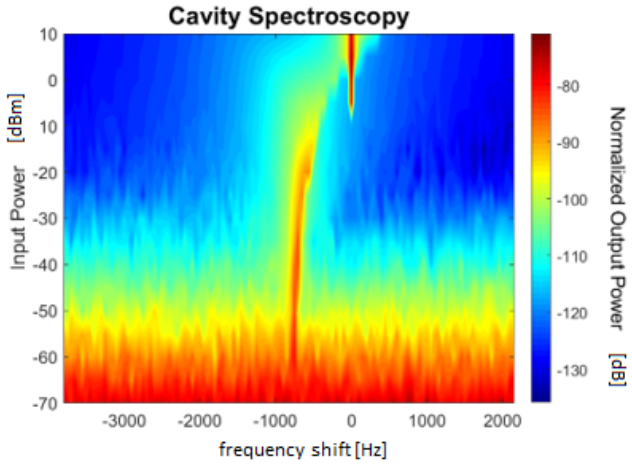

Figure 4: Dispersive Shift. Output power has been normalized with respect to the input power to improve the readout operation.

The state of the qubit can be driven sending through the cavity microwave pulses having certain pattern and duration whose carrier frequency equals the resonance frequency of the qubit. This technique is used in order to study some characteristic features of the qubit itself as the times T_1 and T_2. The former is the time after which the qubit returns spontaneously to the ground state once it has been brought to the excited state by applying a so called π pulse. The latter is the time for which the state remains coherent, during what is called free evolution, after being driven by a $\frac{\pi}{2}$ pulse to a given superposition of the eigenstates like, for instance, $\frac{1}{\sqrt{2}}(|0\rangle + i\,|1\rangle)$.

The qubit inside the cavity exchanges photons with the cavity itself. Photons are alternately emitted and reabsorbed by the qubit that switches its state as the electrons of an atom, whose energy varies among a quantized levels set exchanging radiation quanta with an electromagnetic field. As time goes on the state function of a qubit experiences oscillations between the two eigenstates known as *Rabi Oscillation*.

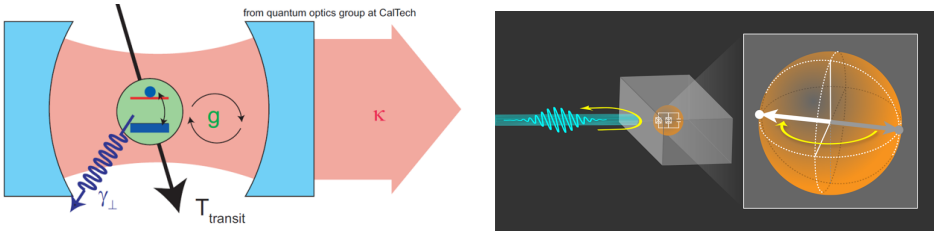

(a) Rabi Cycle. (b) MW Pulse.

Figure 5: Cavity and Qubit system. Photons are exchanged at a rate g while κ is the decaying constant of the field inside the cavity. The MW Pulse drives the state of the qubit inside the cavity.

Of course, when measured, the qubit can only be found to be in one of the two eigenstates. Nevertheless if the measurement is repeated for every pulse length and statistics is applied an oscillation pattern can be observed for the probability function P_e. This function expresses the probability that, at a given time, the qubit is found to be in the excited state. Observe Rabi Oscillations is currently one of the main purpose of the Quantum Computing research group at Fermilab because it allows to get information about the coherence time of the qubit they work with. The coherence time being the time for which the state of a quantum system remains coherent before the interaction with the environment affects the state itself.

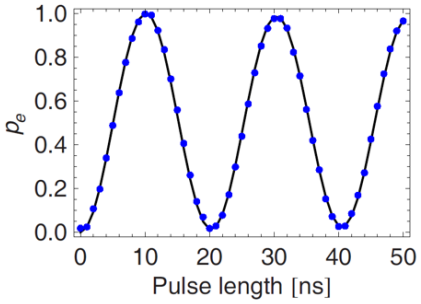

Figure 6: Rabi Oscillations of the probability function P_e.

It is possible to show that the probability function that undergoes Rabi oscillations is related to the phase shift that the system made by both the cavity and the qubit introduces to an injected signal. Thus, reading the transmitted wave at the output of the cavity and measuring the phase shift with respect to the incident wave, we are able to observe the Rabi oscillation pattern we look for.

The task I was assigned to is therefore to design and implement a digital system able to measure the phase difference between two sine wave signals in order to observe Rabi oscillations. The system is required to be digital mostly because it allows data to be processed fast which is a very important feature since repeated measurement undergoing statistical analysis are needed in this context. In a dig-

ital system data would also be available for a real time reading by means of a user interface and, in addition, the possibility of changing certain features of the system modifying only its firmware instead of the hardware is an advantage.

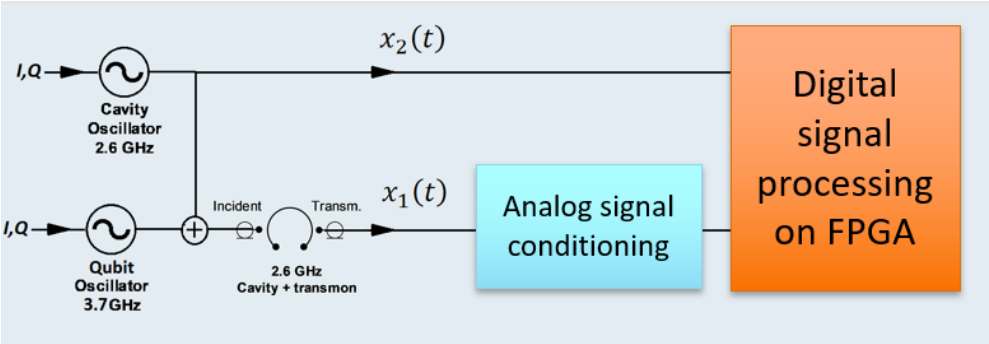

Figure 7: Readout of the cavity and set up for the phase shift measurement. Transmitted wave is labeled as $x_1(t)$ while the incident wave is referred to as $x_2(t)$.

2 System Design

For the setup we have been working with the *digitizer* plays a central role. This instrument can receive analog input signals that are converted into numerical sequences, its sampling frequency being $f_s = 500\,MHz$, and then processed by the FPGA inside the instrument itself. The output of the digital signal processing is then converted into an analog waveform that can be read with any other instrument.

Figure 8: Keysight M3302A Digitizer and Arbitrary Waveform Generator.

To achieve a given system which allows to perform a set of operation on the input data the FPGA inside the digitizer needs to be programmed. This requires codes for the description of the hardware to be written. Hardware description codes can be managed in Vivado which is an environment that allows the user either to write and to simulate a given system observing the time evolution of the input and output waveforms. These codes are then embedded in the FPGA design environment Keysight M3602A that drives the synthesis of the FPGA loading a specific firmware in the digitizer. Once the hardware is ready it can be tested supplying input signals produced by a waveform generator and reading the output of the system with an oscilloscope.

The digitizer I have been using to accomplish my task was part of the new equipment in the Quantum Computing Laboratory so that the entire staff had to get familiar with this instrument and the software environment it works with. As a consequence, part of my task was to test this device in order to fix basic issues and to figure out how to deal with more complex ones. Some of them have been identified and reported to the overall group being still under investigation in order to improve the performance of the system and to have it working properly for future tasks.

2.1 Hardware Design

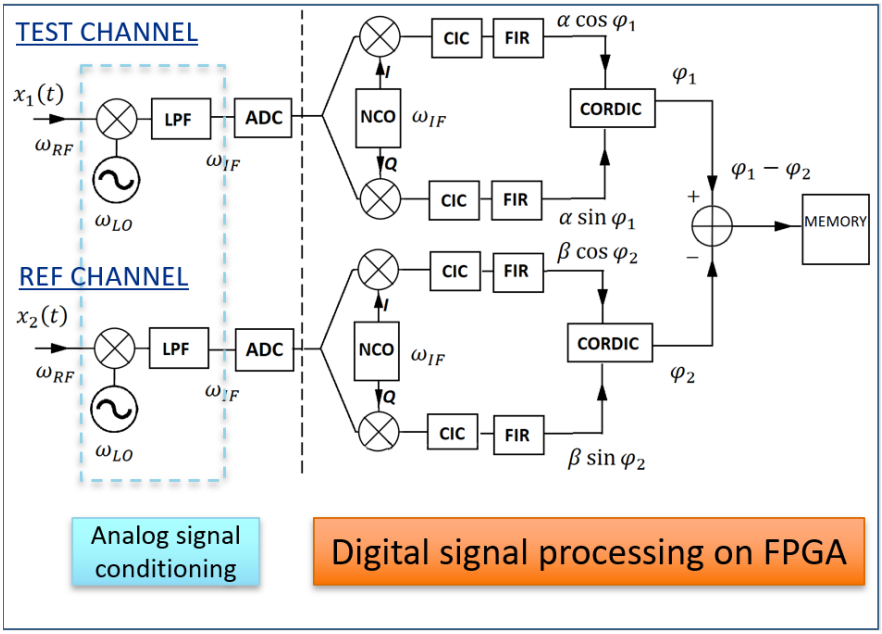

Figure 9: Hardware Schematic of the overall system.

The schematic shown in Fig. 9 summarizes the hardware that has been designed for this system. Here we read on two separate channels the incident and transmitted wave coming from the cavity that are assumed to be the sine wave signals $x_1(t)$ and $x_2(t)$ having the same frequency but different phases at time $t = 0$. For both channels the instantaneous phase is calculated applying a set of operations that are similar to the ones typically used by the receiver of a telecommunication system where an antenna receives a signal that is downconverted to read its in-phase and quadrature components [5]. Once the phases have been calculated they are subtracted to obtain the relative phase shift where it is understood that the incident wave is taken as a reference.

Let us first consider a generic modulated real valued signal $x(t)$ in order to show what is meant with *in-phase* and *quadrature* components of a signal. Since $x(t)$ takes real values and it has been modulated its spectrum has well defined parity properties and it is spread around the carrier angular frequency ω_0. It is therefore convenient to introduce a complex valued signal, whose name is complex modulation envelope or complex baseband equivalent, which brings the same information of $x(t)$ and whose spectrum is contiguous to the origin [6]. We refer to this signal using the symbol $\underline{x}(t)$, its definition being[2]

[2]Imaginary unit in the expressions of the present section follows the convention used in the references. The symbol i was previously used while here we use j. In general both notation can be applied but one has to keep in mind that the two symbols are the roots of the equation $z^2 + 1 = 0$, $z_1 = +\sqrt{-1} \equiv i$ and $z_2 = -\sqrt{-1} \equiv j$ so that they are not equal.

$$\underline{x}(t) = e^{-j\omega_0 t}\mathscr{F}^{-1}\{2u(\omega)X(\omega)\} = x_I(t) + jx_Q(t), \tag{5}$$

where $u(\omega)$ is the Heaviside step function in the angular frequency domain and $\mathscr{F}$ is the Fourier transform operator. The operations specified in the above definition just cancel the negative contribution of the spectrum and shift the result toward the base band leaving the subtended area unchanged. The real and the imaginary part of $\underline{x}$ are, respectively, the in-phase x_I and quadrature x_Q component of $x(t)$. They allow us to express the original signal in the simple following way

$$x(t) = \mathrm{Re}\{\underline{x}(t)e^{j\omega_0 t}\} = x_I(t)\cos(\omega_0 t) - x_Q(t)\sin(\omega_0 t). \tag{6}$$

It is useful to point here that a sine wave having the form $x = A\cos(\omega_0 t + \varphi)$ has a complex envelope $\underline{x} = Ae^{j\varphi}$ its in-phase and quadrature component being respectively $x_I = A\cos\varphi$ and $x_Q = A\sin\varphi$.

Referring back to the schematic of Fig. 9 the processing experienced by one of the input signal, say x_1, can be explained in order to highlight how the system works. Both the input channels are subjected to the same set of operations because of the symmetry of the schematic. The input signal comes from the cavity and, as shown in Fig. 4, it is expected to be a very low power radio frequency signal. Before sampling occurs an analog signal conditioning is applied. First the signal needs to be amplified by a low noise amplifier in order to simplify the readout operation. Then, by means of a mix with a sine wave followed by a low pass filter (LPF), the carrier frequency of the input signal is lowered in order to allow the sampling at given rate. This latter operation is known as downconversion. The spectrum of the signal after the downconversion is spread around an intermediate angular frequency ω_{IF}, its in-phase and quadrature component being unchanged except for halving their amplitudes. The signal is then turn into a numeric sequence by sampling and it starts the digital processing.

A Numerically Controlled Oscillator (NCO) produces two sine waves with angular frequency ω_{IF} being $\pi/2$ out of phase. They both are mixed with the incoming sequence. When a signal whose spectrum is spread around a given angular frequency is multiplied by a sine wave having angular frequency ω_{IF} two replicas of the original spectrum are obtained, one is raised and one is lowered by an amount equal to ω_{IF}. Since the central angular frequency of the incoming signal is ω_{IF} we expect to obtain one spectral replica around the zero frequency and the other one around $2\omega_{IF}$. The former contains the information we are interested in and therefore, by low pass filtering, the higher frequency component is dropped. When the incoming sequence is a cosine signal oscillating at ω_{IF}, as the one we are assuming to receive, after the filtering we should ideally have $\frac{A_1}{4}\cos\varphi_1$ on the I-branch and $-\frac{A_1}{4}\sin\varphi_1$ on the Q-branch. Nevertheless, in the practice, the frequency of the oscillator will not equal exactly the one of the in-

coming sine wave. Thus the output of the mixer will produce a 'slow' sine wave at $\omega_1 = \omega_{IF} - \omega'_{IF}$ and a faster one oscillating at $\omega_{IF} + \omega'_{IF}$, assuming that ω'_{IF} is the angular frequency of the signal produced by the NCO and moreover that $\frac{\omega_{IF}-\omega'_{IF}}{\omega_{IF}} \ll 1$. The latter sine wave is canceled by the filter whose actual output is

$$y_I^{(1)} = \frac{A_1}{4}\cos(\omega_1 t + \varphi_1) \qquad\qquad y_Q^{(1)} = -\frac{A_1}{4}\sin(\omega_1 t + \varphi_1), \tag{7}$$

respectively on the I-branch and the Q-branch.

The low pass filter in the digital system is achieved as the cascade of a CIC filter and a FIR filter. The former, whose acronym stands for *Cascaded Integrator-Comb* filter, is a type of digital filter that acts both as a downsampler, reducing the sampling frequency, and as a notch filter allowing to place almost arbitrary roots in the frequency response. The CIC is obtained by the repetition of its basic cell which is composed by an integrator stage and a comb stage [7]. The integrator section of a CIC filters consists thus of, say, N digital integrator stages operating at the high sampling rate f_s. Each stage is implemented as a one-pole filter with a unity feedback its response being $H_I(z) = \frac{1}{1-z^{-1}}$. The comb section operates with the reduced sampling frequency f_s/R and each stage consists in a delay block introducing a delay of M samples, its response being $H_C(z) = 1 - z^{-RM}$.

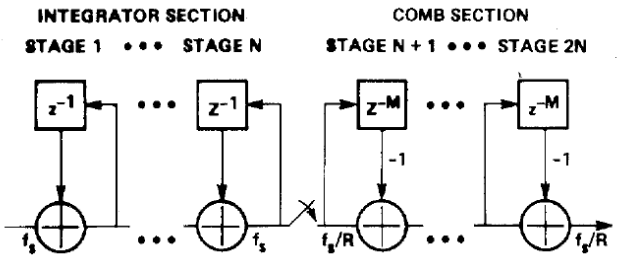

Figure 10: CIC decimation filter.

The response of the overall N-stages filter is then

$$H(z) = H_I^N(z)H_C^N(z) = \frac{(1-z^{-RM})^N}{(1-z^{-1})^N}, \tag{8}$$

which has to be evaluated at $z = e^{j2\pi f/f_s} = e^{j2\pi\frac{\nu}{R}}$ where $\nu = \frac{f}{f_s/R}$ is the frequency normalized with respect to the lower sampling rate. This yields

$$H(\nu) = e^{-jN(M-\frac{1}{R})\pi\nu}\left[\frac{\sin(M\pi\nu)}{\sin(\pi\nu/R)}\right]^N \approx e^{-jMN\pi\nu}\left[RM\frac{\sin(M\pi\nu)}{M\pi\nu}\right]^N, \tag{9}$$

where, on the right side, the approximation for large reduction factor $R \gg 1$ has been taken into account. The CIC filter is therefore understood to be a linear

phase filter whose roots are easily specified by (9) their sharpness being increased by an increasing number of stages.

A *Finite Impulse Response* (FIR) filter of n-th order is one whose impulse response is specified by a set of $n+1$ samples being, in addition, the coefficients of the polynomial which corresponds to the filter response. Conversely to the CIC filter the FIR exhibit less oscillations in the frequency response which can stay flat for a broad frequency range having uniform attenuation. The FIR filter has not been included in the actual project but it should be taken into account for the performances to be improved. The benefit of a broader filtering would be to cancel any higher frequency residual and to compensate possible effects due to the finite bandwidth of the received signal. Moreover the angular frequency of the input signals can vary depending on the qubit being in the ground state or in the excited state so that the root introduced by the CIC filter will not always occur at an optimal frequency value. Finally mechanical resonant phenomena, as the activity of the vacuum pump in the cryomodule, couple to the cavity resonance modulating the amplitude of the corresponding signal. As a consequence of this phenomenon, which is known as *cavity microphonics*, the spectroscopy measurement can exhibit two side lobes in addition to the resonant peak associated to the mode of the cavity itself.

Once quantities in (7) have been calculated they can be used to obtain the time varying common argument by applying the so called CORDIC algorithm. Its name stands for *COordinate Rotation DIgital Computer*. It establishes an isomorphism with a two dimensional vector space that allows to calculate an angle once its cosine and sine are given. The cosine and the sine functions are understood to be the rectangular component of the corresponding vector that can be represented on a plane using a Cartesian coordinate system. Thus the actual output of the CORDIC block on the test channel we are considering will be the argument function $\theta_1(t) = -(\omega_1 t + \varphi_1)$. Once the CORDIC algorithm has been applied on both channels, by subtraction we obtain the relative phase shift we wanted to measure that is

$$\theta_2(t) - \theta_1(t) = \varphi_1 - \varphi_2. \tag{10}$$

2.2 Intermediate Blocks Test

Before to exhibit the results achieved for the overall system the ones obtained for some prior fundamental blocks are shown and the details of some test operations are discussed. If the reader is only interested in the results concerning the overall system, this part can be skipped and he/she can go directly to the following section.

Let us start this part from the design of the CIC filter whose role and working

principles have been previously discussed. A test for this component can be obtained using the following hardware.

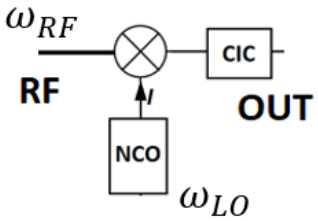

Figure 11: Hardware for CIC filter block test.

In the hardware shown in Fig. 11 a sine wave oscillating at $f_{LO} = \frac{\omega_{LO}}{2\pi} = 27.8$ MHz is produced by a Numerical Controlled Oscillator and mixed with an arbitrary input signal which is fed from the waveform generator, its spectrum being spread around a given f_{RF} frequency. As it has been already pointed, the mixer gives rise to spectral replicas whose center frequencies are $f_{RF} - f_{LO}$ and $f_{RF} + f_{LO}$. The CIC filter here is designed to retain only the low frequency component produced by the mixing operation. The test has been carried with the input signal $x_{RF} = \cos(\omega_{RF}t)$ where $f_{RF} = \frac{\omega_{RF}}{2\pi} = 27.522$ MHz. Thus the output of the mixer is found to be $\cos(\omega_{RF}t)\cos(\omega_{LO}t) = \frac{1}{2}\cos(\omega_{RF} - \omega_{LO})t + \frac{1}{2}\cos(\omega_{RF} + \omega_{LO})t$ where the second term is to be canceled.

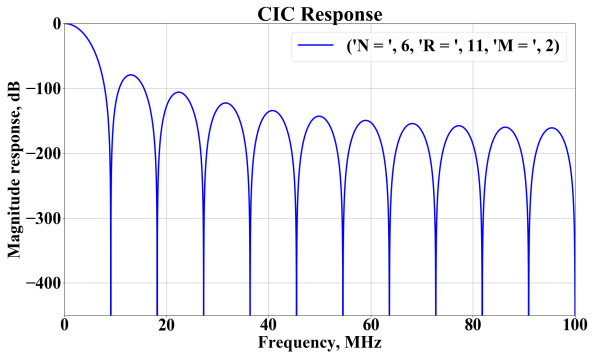

Figure 12: Frequency Respnse of CIC filter. Magnitude in logarithmic units. The design parameters have been displayed following the notation previously introduced and being N=6, R=11, M=2 and $f_s = 200$ MHz.

From the frequency response of the CIC filter in Fig. 12 it can be verified that the sum frequency $f_{RF} + f_{LO} = 55.322$ MHz receive enough attenuation and thus it is filtered. Since we are interested in reading the low frequency component of the mixer output it is useful to show with more details the low frequency response of the filter. In addition this is compared with the one measured with a Vector Network Analyzer (VNA) showing a good match with the simulation.

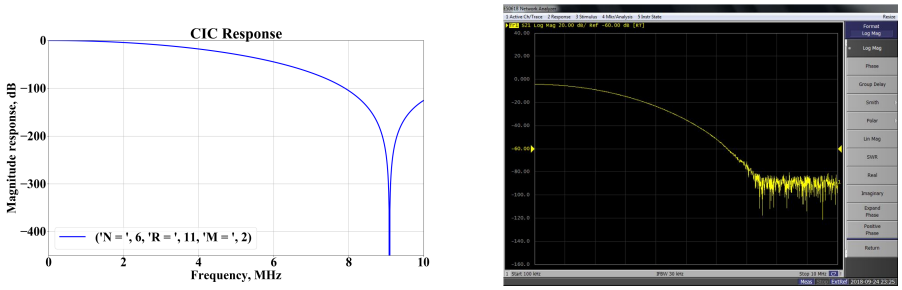

(a) Simulation. (b) VNA Measurement.

Figure 13: Low frequency response of the designed CIC filter. Up to 10 MHz

The filter behavior is then verified reading the output of the system with an oscilloscope. As it can be predicted by the trigonometric identity previously written, a sine wave having the slower frequency $f_{RF} - f_{LO} = 278$ kHz is obtained.

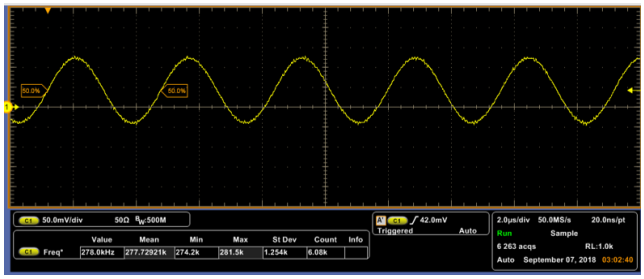

Figure 14: Output of the CIC filter with a sine wave input oscillating at $f_{RF} = 27.522$ MHz. A 278 kHz sine wave is obtained.

One further block for which intermediate tests will be exhibited is the one that applies the CORDIC algorithm. The hardware implemented for the current test has been shown below.

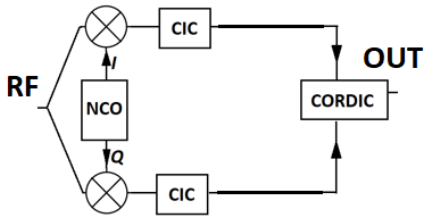

Figure 15: Test of the CORDIC block. Hardware Schematic.

An input signal is received from the waveform generator and is mixed with the $\pi/2$ out of phase sine waves produced by an NCO. The mixed waveforms are filtered before being fed as input signals of the CORDIC in order to retain only the low frequency contribution resulting from the mix. It may be noticed that the steps listed above are similar to the ones applied when testing the CIC filter but

this time two signal has been produced in order to detect the phase of the input RF sine wave where the NCO has been used as a reference. Likewise the previous test the input is a sine wave whose frequency is $f_{RF} = 27.522$ MHz while the signals from the NCO oscillate at $f_{RF} = 27.8$ MHz. The input of the CORDIC block are thus $\frac{1}{2}\cos(\omega_{RF} - \omega_{LO})t$ and $-\frac{1}{2}\sin(\omega_{RF} - \omega_{LO})t$. The common time varying argument to be detected is then $\theta(t) = -[(\omega_{RF} - \omega_{LO})t + \theta_0]$, where θ_0 is the phase of the input signals at time $t = 0$. The output of the tested system is therefore a linearly decaying ramp, its values being forced by the algorithm itself to be bounded in a range corresponding to $[-\pi, \pi)$ angles.

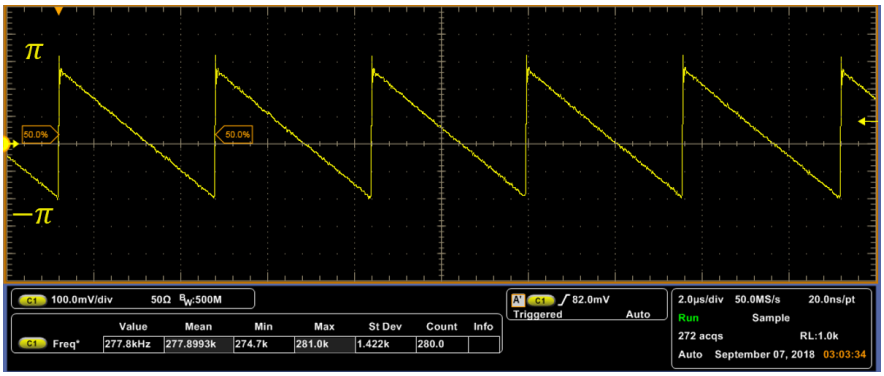

Figure 16: Test of the CORDIC block. Output signal.

3 System Implementation and Tests

In this section the overall system is implemented following the design explained in 2.1. The final project has been achieved by means of a single hardware description code where all the components corresponding to the fundamental blocks of the system are defined together with the mapping of the internal connections among them. Before being implemented on the actual FPGA board the system has been simulated using what in VHDL environments is called a *test bench*. Let us first discuss the result of this simulation.

The following system parameters have been used for the components shown in the hardware schematic of Fig. 9.

- Frequency of the input signals, numerically generated in the simulation, $f_{IF1} = f_{IF2} \equiv f_{IF} = 27.522$ MHz.
- Frequency of the sine waves produced by the actual NCO, f'_{IF}.
- Parameters for CIC low pass filter: N=6, R=11, M=2. Details concerning their meaning and the response of the filter itself can be found in section 2.1.
- System clock frequency, driving all the components, $f_{CK} = 200$ MHz.

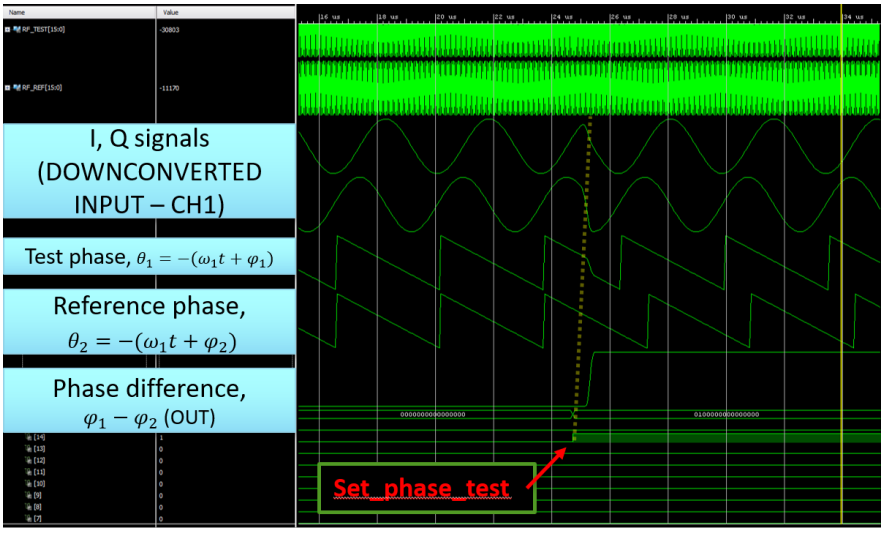

Figure 17: Test bench of the system. Waveform are represented in time domain to observe its behavior.

Following the label in the figure, signals belonging to different stages of the system are represented. The low frequency sine waves labeled as "Downconverted input - CH1" are the output of the CIC filters lying in the test channel side. They are fed to the subsequent CORDIC block to produce the "Test phase, θ_1" signal.

The same operation is done in the reference channel side to achieve the waveform labeled as "Reference phase, θ_2". By subtraction the required phase difference $\varphi_1 - \varphi_2$ is obtained. For this simulation a control signal has been introduced, whose name is "Set phase test", in order to force an arbitrary value for φ_1 which is the phase of the test input signal at time $t = 0$. Default values for those angles are chosen to be $\varphi_1 = \varphi_2 = 0$ so that if the control signal is set to be zero we observe zero phase difference too. If at some given time the control signal is raised it introduces an abrupt phase change resulting in a non-zero phase difference, as it is shown in the simulation.

3.1 Test and Measures

Results for the actual system, once the corresponding firmware has been loaded in the digitizer, are now shown. In the first test we send two monochromatic waves into the input channels of the digitizer having the same frequency and a given phase shift. According to the behavior of the system and to the simulation previously discussed the output is a constant signal whose value is proportional to the relative phase shift of the input signals.

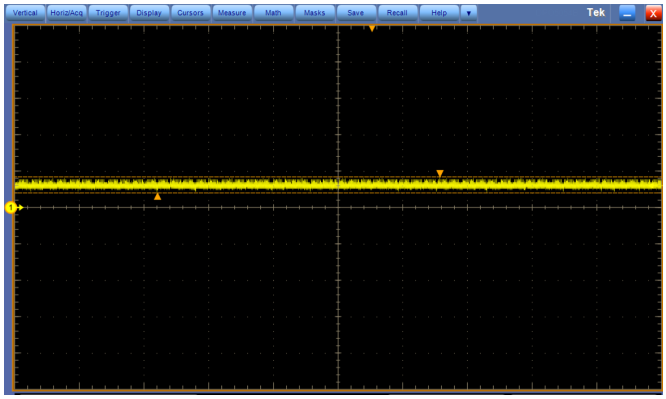

Figure 18: Test of the implemented system. Phase difference measurement.

A further interesting test can be exhibited applying a phase modulation. The process of Phase Modulation (PM) is often employed in the field of communication when a signal is transmitted as the variation of the instantaneous phase of a sine wave carrier. If $m(t)$ is the signal representing the message to be encoded and ω_0 is the angular frequency of the carrier, the phase modulated signal being transmitted takes the form

$$x(t) = A\cos(\omega_0 t + m(t)). \tag{11}$$

In the following test a square wave signal modulates the phase of the input waveform coming from the first channel. Thus, when its phase is detected and subtracted to the one belonging to the reference channel which is a constant, the

output of the system is, apart from a static offset, the modulating square wave signal itself. This result is displayed in the following readout achieved with the oscilloscope. The blue trace is the modulated signal which is described by (11). Its phase has been modulated by a square wave that abruptly changes its level between two values and thus discontinuity effects are visible. The yellow trace is the modulating wave that the system is able to detect after some delay.

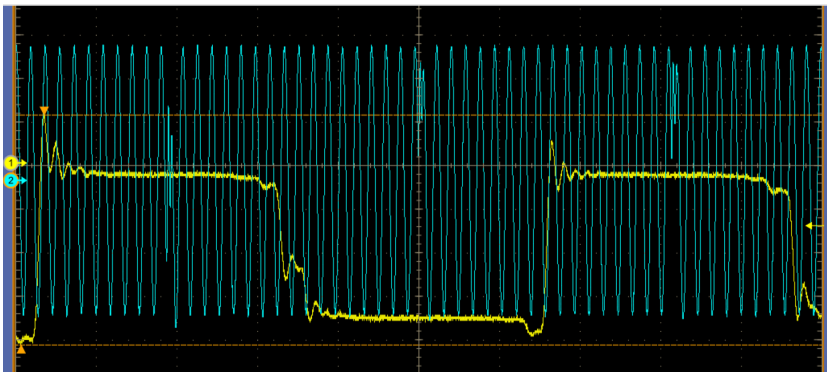

Figure 19: Test of the implemented system. Detection of the modulated signal, yellow trace, in a phase modulation.

The delay of a digital system is an important features of the system itself. Thus a measurement of the *latency*, that is the time after which the system responses once the stimulus has been sent, is given. We want to know the latency of our system because it gives an estimate about how fast it can be. One way to measure this quantity is to send a pulsed signal on the test channel of the system and then read the time elapsed before a change in the phase difference occurs.

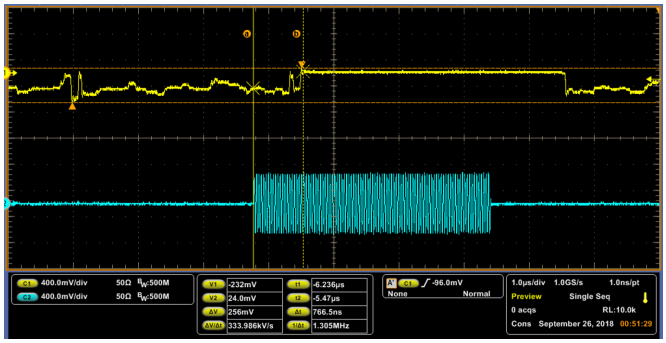

Figure 20: Test of the implemented system. Measure of the latency by bursts sent in the first channel.

As it appears in Fig. 20, the output waveform takes well-defined values only while the pulses are active displaying just phase noise when they are turned off. Markers are placed on the screen in order to show the latency time whose value is $\tau_L = 766.5$ ns, which states that our system is fast enough.

3.2 Criticalities of the System

It was previously mentioned that both the hardware system and the software environment it works with are new instrument installed in the Quantum Computing laboratory. Therefore, during the development of this project, it has been necessary to figure out most of the features of this equipment in order to have the designed system blocks working. Both basic and complex issues have occurred during the implementation of this system and here the main drawbacks among the ones identified are highlighted. Those weaknesses, being reported to the research group, are still under investigation in order to improve the performance of the system.

A first issue concerns the representation of the data. The full capacity of the digitizer allows to work with a five channels parallel stream having 100 MHz speed each. It was observed that data are properly represented only if the full capacity of the channels is used but this would require the registers to be too large, 80 bit width, which is really inconvenient. It would be preferable to work with reduced width registers, saving hardware resources, and higher clock frequencies. For this project we have been working with a single 16 bit channel whose clock run at $f_{CK} = 200$ MHz. These settings do not match correctly the trigger operating mode of the software so that the numerical signals undergo incorrect representation and low pass filters are needed in order to display clean waveforms on the oscilloscope avoiding aliasing effects.

As previously said it would be useful to include a user interface for this system so that results could be observed directly and external controls could be set easily. This would basically require to read and write data to registers. Nevertheless in the software environment associated with the digitizer it was not intuitive to understand how it is supposed to be done and it still needs to be understood.

Furthermore, the CORDIC algorithm provided by the software, available as a Vivado IP (*Intellectual Property*), has not worked properly so that it was necessary to include in the project another code for the same algorithm that was available from previous works made in the Quantum Computing Lab. The CORDIC provided by Vivado still needs a calibration in order to have a well-defined reading for the phase difference. In fact, since phases are represented in the $[-\pi, \pi)$ interval by adding jumps of amplitude 2π, the difference takes incorrect values at some given times. This is illustrated in the Matlab plot that follows.

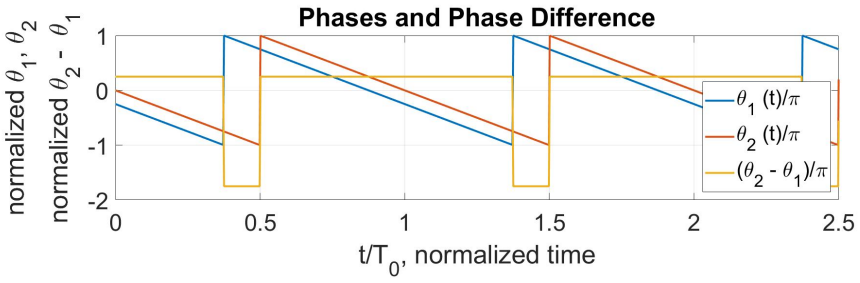

Figure 21: Phase representation criticalities. Blue and red traces are argument of coherent sine waves, the yellow one being their difference.

It can be observed that at first the phase difference trace takes one value that is supposed to be the correct one. Then, because of their relative delay, one argument receive the 2π offset before and the phase difference is consequently subjected to the same offset until the delayed argument experiences, in turn, the 2π jump.

Conclusions

Here it follows a brief resume of the main achievements of the work I have done during my internship in the Applied Physics and Superconductive Technology Division at Fermilab.

The new instrument has been installed in the laboratory and it was figured out how to synthesize a given project with this equipment even if some weaknesses, pointed in section 3.2, still need to be improved. The digital system for the phase difference measurement is now implemented and has shown good results when test operations were performed. Once the highlighted criticalities will be solved this system could be included in the instrumentation test bench for the characterization of a Qubit in the Quantum Computing Laboratory.

I would like to thank Fermilab for the great cultural experience I had during my staying in the United States. I would especially like to address my thanks and gratitude to the colleagues of the division I joined for the learning and the good times we had working together. One more thanks to my supervisors Silvia, Danil and Roman for the teaching, the wise advice and the support they have been giving to me in the laboratory.

October 2018

References

[1] I. Djordjevic, *Quantum Information Processing and Quantum Error Correction.* Academic Press, 2012.

[2] B. Bransden and C. Joachain, *Quantum Mechanics, Second Edition.* Pearson, 1999.

[3] J. Gambetta, A. Blais, D. I. Schuster, A. Wallraff, L. Frunzio, J. Majer, M. H. Devoret, S. M. Girvin, and R. J. Schoelkopf, "Qubit-photon interactions in a cavity: Measurement-induced dephasing and number splitting," *Phys. Rev. A*, vol. 74, p. 042318, Oct 2006.

[4] A. Blais, R.-S. Huang, A. Wallraff, S. M. Girvin, and R. J. Schoelkopf, "Cavity quantum electrodynamics for superconducting electrical circuits: an architecture for quantum computation," *Physical Review*, vol. A, 2004.

[5] D. M. Pozar, *Microwave Engineering, Fourth Edition.* Wiley, 2011.

[6] D. Tse and P. Viswanath, *Fundamentals of Wireless Communication.* Cambridge University Press, 2005.

[7] E. Hogenauer, "An economical class of digital filters for decimation and interpolation," *IEEE Transactions on Acoustics, Speech, and Signal Processing*, vol. 29, 1981.